Acta Mechanica 187, 75–83 (2006)
DOI 10.1007/s00707-006-0367-y

Acta Mechanica
Printed in Austria

Vortex breakdown generated by off-axis bifurcation in a cylinder with rotating covers

A. V. Bisgaard, **M. Brøns** and **J. N. Sørensen**, Kongens Lyngby, Denmark

Received January 9, 2006; revised April 28, 2006
Published online: August 3, 2006

Summary. Vortex breakdown of bubble type is studied for the flow in a cylinder with rotating top and bottom covers. For large ratios of the angular velocities of the covers, we observe numerically that the vortex breakdown bubble in the steady regime may occur through the creation of an off-axis vortex ring. This scenario does not occur in existing bifurcation theory based on a simple degeneracy in the flow field. We extend the theory to cover a non-simple degeneracy, and derive the associated bifurcation diagrams. We show that the vortex breakdown scenario involving a vortex ring can be explained from this theory, and that the numerically generated bifurcation diagrams are consistent with the theory.

1 Introduction

The term *vortex breakdown* is used to describe abrupt spatial changes in the structure of a vortex. This much studied phenomenon was first reported by Peckham and Atkinson [19] in connection with the flow over delta wings. Several different types of vortex breakdown have been identified. The main categories are the *S-type*, where the vortex changes into a spiral structure, and the *B-type*, where a recirculating zone (or bubble) attached to the vortex axis appears [15].

A much used set-up for the study of vortex breakdown is a fluid-filled cylinder where a swirling flow is generated by rotating covers. The system parameters governing the flow are the cylinder aspect ratio $h = H/R$, the Reynolds number $Re = \Omega_1 R^2/\nu$, and the ratio of the angular velocity of the covers $\gamma = \Omega_2/\Omega_1$. Here R and H are the radius and height of the cylinder, Ω_1 and Ω_2 are the angular velocities of the rotating bottom and top cover, and ν is the kinematic viscosity of the fluid. Experiments by Vogel [28], Ronnenberg [20], and Escudier [11] with a fixed top cover and a rotating bottom cover, corresponding to $\gamma = 0$, show that up to several vortex breakdowns of B-type may be formed at the center axis. Escudier [11] also established a bifurcation diagram in the parameter domain $1.0 < h < 2.5$ and $1000 < Re < 3000$, mapping the transitions between the different flow topologies. The location and shape of the vortex breakdown bubbles have been reproduced accurately from numerical simulations assuming axisymmetry of the flow [17], [22], even if the details of the structure of the breakdown bubble are sensitive to three-dimensional imperfections [23], [25], [26]. The structure of vortex breakdown bubbles for non-zero values of γ has been studied both experimentally and computationally in [1], [3], [6], [12], [18], [27]. These studies show that the flow topology is quite sensitive to variations in γ.

B-type vortex breakdown also occurs if the top cover is removed, and the fluid has a free surface [24]. This configuration has been proposed as an easily controllable layout for a

bioreactor [10]. The effects of magnetic fields on the flow of a liquid metal are studied in [2]. Furthermore, for high values of the aspect ratio h, S-type vortex breakdown has recently been observed [16], [21], demonstrating the richness of this simple flow configuration.

In the parameter regime we consider here, there is a unique, steady stable flow. Hence, changes in the flow pattern are not associated with any dynamical instability, but are solely associated with a change in the topology of the flow field as the parameters are varied, and for each set (h, Re, γ) there is a unique flow topology. Such topological changes are conveniently described with terms from non-linear dynamics. Vortex breakdown of B-type normally occurs by the creation of a degenerate stagnation point (or critical point) on the vortex axis. As parameters are changed, the degenerate stagnation point turns into two regular, nearby stagnation points of saddle type. The bubble surface consists of a stream surface connecting one stagnation point to the other. Thus, as the stagnation points move away from one another, the breakdown bubble grows in size. The dynamical systems approach has successfully been used to construct bifurcation diagrams from numerical simulations in the steady, axisymmetric domain [3]–[8]. The analysis is based on theoretically obtained bifurcation diagrams which describe the possible flow topologies close to degenerate stagnation points where the linearization of the velocity field has a zero eigenvalue. If the geometric multiplicity of the zero eigenvalue is one, the degeneracy is denoted *simple*. Theoretical bifurcation diagrams for simple stagnation points are constructed in [5], and they have been sufficient to explain all hitherto observed topological changes associated with bubble-type vortex breakdown for low values of γ. However, for higher values of γ than previously analyzed systematically, sequences of bifurcations occur which cannot be described by the bifurcation theory of simple stagnation points.

An example is shown in Fig. 1. Here stagnation points are created off-axis together with a vortex ring. The change in topology from no breakdown (Fig. 1a) to breakdown (Fig. 1e) occurs in two stages. First a degenerate stagnation point is created off-axis (Fig. 1b), and the stagnation point bifurcates into a regular saddle and a regular center (Fig. 1c). The dividing streamline of the saddle point defines a vortex ring. The vortex ring attaches to the axis in a degenerate stagnation point (Fig. 1d), and a breakdown bubble is finally created (Fig. 1e). Vortex rings as in (Fig. 1c) and degenerate configurations as in (Fig. 1d) do not occur in bifurcation diagrams based on simple eigenvalues. Hence, a new theoretical framework is needed to topologically describe the transitions shown in Fig. 1.

In the present paper, we provide this framework by performing a bifurcation analysis for a non-simple stagnation point at a vortex axis. We show that the existence of vortex rings is to be expected near non-simple degenerate stagnation points, and that the bifurcation scenario in Fig. 1 appears in the bifurcation analysis. We perform numerical simulations for γ in a region not analyzed in detail before, and show that non-simple stagnation points occur consistently. We construct two-dimensional bifurcation diagrams in the (h, Re) plane, and show that the range where vortex rings occur may be quite large.

2 Bifurcation of flow structures near a non-simple degeneracy

Consider an incompressible, axisymmetric flow described in cylindrical coordinates (r, θ, z) with corresponding velocity components (u, v, w). The velocity field depends only on r, z, and a stream function $\psi(r, z)$ exists such that

$$u = \frac{1}{r}\frac{\partial \psi}{\partial z}, \quad w = -\frac{1}{r}\frac{\partial \psi}{\partial r}. \tag{1}$$

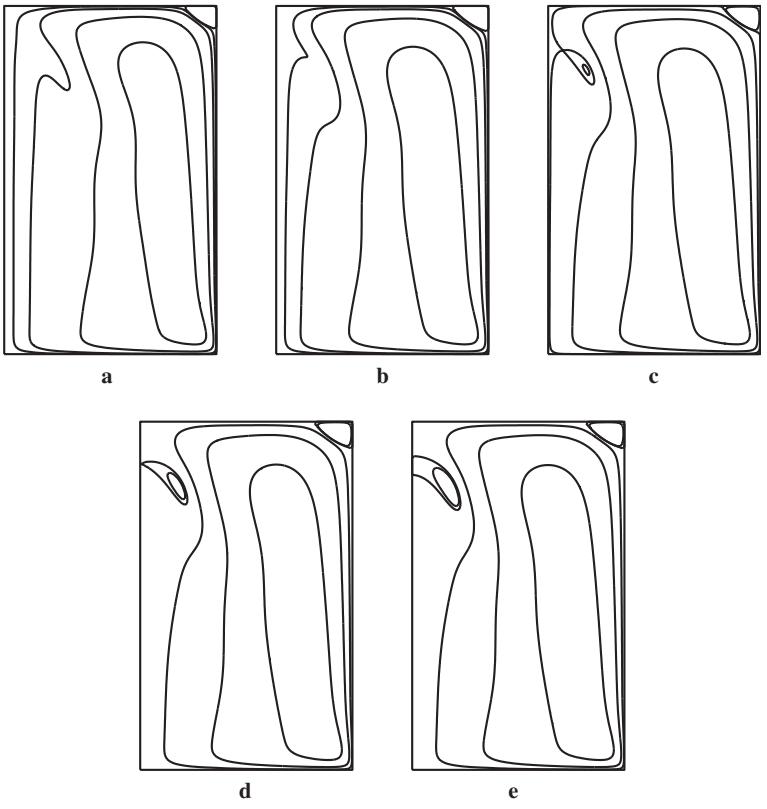

Fig. 1. Sample patterns of the steady flow in the cylinder for different values of the system parameters. Each panel shows intersections of the axisymmetric stream surfaces in a meridional plane. Only the right half of the meridional plane is shown. The vertical line to the left is the cylinder axis. The curves are obtained as iso-curves of the stream function ψ using the finite-difference code described in Sect. 3. In all cases $\gamma = 0.14$, $h = 1.64$. **a** $Re = 2400$, no secondary flow structure; **b** $Re = 1933.3$, off-axis degenerate stagnation point; **c** $Re = 1875$, an in-flow vortex ring; **d** $Re = 1853.8$, the vortex ring attaches to the center axis at a degenerate stagnation point; **e** $Re = 1825$, vortex breakdown bubble

The center axis is a streamline, so a boundary condition is

$$\psi = 0 \quad \text{for } r = 0. \tag{2}$$

Introducing a new radial variable $\rho = \frac{1}{2}r^2$ the differential equations for the iso-curves of ψ are recast into the two-dimensional Hamiltonian system

$$\dot{\rho} = ur = \frac{\partial \psi}{\partial z}, \quad \dot{z} = w = -\frac{\partial \psi}{\partial \rho}. \tag{3}$$

The iso-curves of ψ are intersections of axisymmetric stream surfaces with a meridional plane.

A topological investigation of Eqs. (3) commences by a local analysis conducted close to a given point on the axis. We take this point to be the origin $(\rho, z) = (0, 0)$. The local analysis is based on the expansion

$$\psi(\rho, z) = \sum_{m,n=0}^{\infty} \psi_{m,n} \rho^m z^n. \tag{4}$$

From the boundary conditions (2) we find that

$$\psi_{0,n} = 0 \quad \text{for } n = 0, 1, 2, \ldots. \tag{5}$$

With this, the system (3) becomes

$$\begin{pmatrix} \dot{\rho} \\ \dot{z} \end{pmatrix} = \begin{pmatrix} 0 \\ -\psi_{1,0} \end{pmatrix} + \begin{pmatrix} \psi_{1,1} & 0 \\ -2\psi_{2,0} & -\psi_{1,1} \end{pmatrix} \begin{pmatrix} \rho \\ z \end{pmatrix} + O\Big(|\rho, z|^2\Big). \tag{6}$$

For $\psi_{1,0} = 0$ the origin is a stagnation point. Linearizing at the origin the system has the Jacobian matrix

$$\mathbf{J} = \begin{pmatrix} \psi_{1,1} & 0 \\ -2\psi_{2,0} & -\psi_{1,1} \end{pmatrix}. \tag{7}$$

If $\psi_{1,1} \neq 0$ the Jacobian $\mathbf{J}$ has the simple eigenvalues $\lambda = \pm\psi_{1,1}$ implying that the stagnation point is a hyperbolic saddle having the center axis as one separatrix and a second separatrix points into the flow. Depending on the sign of $\psi_{1,1}$ the saddle is either a point of separation or attachment. If $\psi_{1,1} = 0$ it follows that $\mathbf{J}$ has an eigenvalue $\lambda = 0$ with algebraic multiplicity 2 and the origin is a degenerate stagnation point.

Two sub-cases exist. If $\psi_{2,0} \neq 0$ the zero eigenvalue has geometric multiplicity 1. If $\psi_{2,0} = 0$ the zero eigenvalue has geometric multiplicity 2. The first case is analyzed in detail in [5], and we now consider the latter case.

The parameters $\psi_{m,n}$ are functions of the physical parameters h, Re, γ. We are interested not only in the case where an exact degeneracy $\psi_{1,0} = \psi_{1,1} = \psi_{2,0} = 0$ occurs – corresponding to specific sets of the physical parameters – but also in the changes of the flow pattern when the parameters are close to such a degenerate combination. Hence, we think of $\psi_{1,0}, \psi_{1,1}, \psi_{2,0}$ as small parameters, and to distinguish this, we rename them

$$\varepsilon_{1,0} = \psi_{1,0}, \quad \varepsilon_{2,0} = \psi_{2,0}, \quad \varepsilon_{1,1} = \psi_{1,1}.$$

With this, the stream function reads

$$\psi(\rho, z) = \rho\big(\varepsilon_{1,0} + \varepsilon_{2,0}\rho + \varepsilon_{1,1}z + \psi_{3,0}\rho^2 + \psi_{2,1}\rho z + \psi_{1,2}z^2\big) + O\Big(|\rho, z|^4\Big). \tag{8}$$

This stream function can be simplified by assuming that $\psi_{1,2} \neq 0$, and by introducing a translation along the center axis together with a linear transformation

$$\begin{pmatrix} \rho \\ z \end{pmatrix} = \begin{pmatrix} 0 \\ -\frac{\varepsilon_{1,1}}{2\psi_{1,2}} \end{pmatrix} + \begin{pmatrix} 1 & 0 \\ -\frac{\psi_{2,1}}{2\psi_{1,2}} & 1 \end{pmatrix} \begin{pmatrix} x \\ y \end{pmatrix}, \tag{9}$$

Eq. (8) becomes

$$\psi(x, y) = x\big(\bar{\varepsilon}_{1,0} + \bar{\varepsilon}_{2,0}x + \bar{\psi}_{3,0}x^2 + \psi_{1,2}y^2\big) + O\Big(|x, y|^4\Big), \tag{10}$$

where

$$\bar{\varepsilon}_{1,0} = \left(\varepsilon_{1,0} - \frac{\varepsilon_{1,1}^2}{4\psi_{1,2}}\right), \ \bar{\varepsilon}_{2,0} = \left(\varepsilon_{2,0} - \frac{\varepsilon_{1,1}\psi_{2,1}}{2\psi_{1,2}}\right), \ \bar{\psi}_{3,0} = \left(\psi_{3,0} - \frac{\psi_{2,1}^2}{4\psi_{1,2}}\right).$$

Further assuming that $\bar{\psi}_{3,0} \neq 0$ allows us to introduce the scaling

$$y \to \sqrt{\left|\frac{\bar{\psi}_{3,0}}{\psi_{1,2}}\right|}y \tag{11}$$

and, finally, dividing by $\bar{\psi}_{3,0}$, we arrive at the *normal form*

$$\psi(x, y) = x\big(c_1 + c_2x + x^2 + \sigma y^2\big) + O(|x, y|^4), \tag{12}$$

where c_1 and c_2 are scaled small parameters and $\sigma = +1$ for $\bar{\psi}_{3,0}/\psi_{1,2} > 0$ and $\sigma = -1$ for $\bar{\psi}_{3,0}/\psi_{1,2} < 0$. The normal form (12) leads to the dynamical system

$$\dot{x} = 2\sigma xy, \quad \dot{y} = -(c_1 + 2c_2x + 3x^2 + \sigma y^2), \tag{13}$$

truncated at third order.

The analysis of the system (13) commences by locating the stagnation points. On-axis stagnation points with $x = 0$ satisfy

$$c_1 + \sigma y^2 = 0 \tag{14}$$

with solution $y = \pm\sqrt{-c_1/\sigma}$. Hence, the stagnation points exist when c_1 has the opposite sign of σ, and bifurcation occurs when $c_1 = 0$. Stagnation points off the axis with $x \neq 0$ satisfy $y = 0$ and

$$c_1 + 2c_2x + 3x^2 = 0. \tag{15}$$

The number of stagnation points changes when the discriminant of this equation is zero,

$$c_2^2 = 3c_1. \tag{16}$$

At this parameter combination, the stagnation point has $x = -c_2/3$. It is in the physical domain $x \geq 0$ only for $c_2 \leq 0$. Away from the bifurcation curve (16), there are either two or no stagnation points. The type of the stagnation points can be determined by the determinant of the Jacobian; if it is positive, the stagnation point is a center, if it is negative, it is a saddle [13]. It is not difficult to see that the bifurcation occurring at the curve (16) is the merging and disappearance of a saddle and a center, previously denoted a *cusp bifurcation* [5], [7].

When $\sigma = -1$ four stagnation points exist for $c_2 < -\sqrt{3c_1}$ and $c_1 > 0$; two saddle points on the center axis, one in-flow center and one in-flow saddle point, see Fig. 2a. This constellation of stagnation points gives the possibility of two global topologies. Either a recirculation zone exists together with an in-flow saddle point, or an in-flow homoclinic loop exists together with two separatrices emanating from the center axis. A global bifurcation involving heteroclinic connections between the saddle points separates the two topologies. The global bifurcation curve is determined by using the fact that the value of the stream function at the in-flow saddle point is equal to the value of the stream function on the center axis due to the heteroclinic connections, i.e., Eq. (15) together with

$$\psi(x, 0) = x(c_1 + c_2x + x^2) = 0. \tag{17}$$

Solving these equations and discarding the solution $x = 0$ and $c_1 = 0$, one finds that the global bifurcation takes place at $c_2 = -2\sqrt{c_1}$ for $c_1 > 0$.

This completes the bifurcation analysis, which is summarized in Fig. 2. The sequence of flow topologies shown in Fig. 1 is found for $\sigma = +1$ if $c_2 < 0$ and c_1 is decreased from positive to negative values. This indicates that non-simple degenerate stagnation points may occur for non-zero rotation rates γ. In the next section we show that this is indeed the case.

The above analysis assumes the non-degeneracy conditions $\psi_{1,2} \neq 0$, $\overline{\psi}_{3,0} \neq 0$. If one of these conditions is violated, the natural setting is to consider the parameter as small, and add it as another ε-parameter to the list of small parameters. This will give rise to three-parameter normal forms including terms of higher order in the spatial variables, and corresponding more complex bifurcation diagrams. This analysis is outside the scope of the present paper.

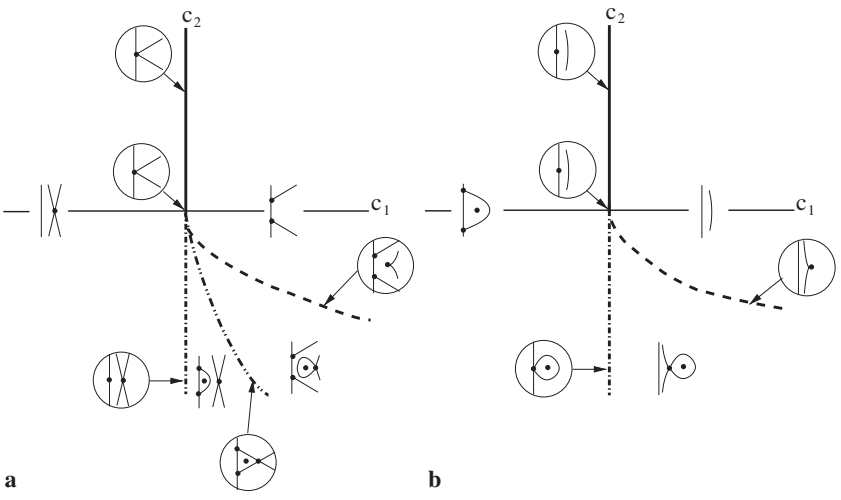

Fig. 2. Bifurcation diagram for the normal form Eq. (12); **a** $\sigma = -1$. **b** $\sigma = +1$

3 Numerically obtained bifurcation diagrams

We have used a vorticity-stream function based finite-difference code to solve the Navier–Stokes equations for the axisymmetric flow in the cylinder. The code was developed at LIMSI/CNRS [9], [22] and has been thoroughly validated against experiments and grid dependence [7], [8], [22]. The grid consists of 100 nodes in the radial direction and $100\,h$ nodes in the axial direction.

A detailed bifurcation analysis in the steady regime for $-0.04 \leq \gamma \leq 0.075$ has been conducted in [3], [4], [6], [7]. Here we consider $0.075 \leq \gamma \leq 0.20$. For fixed values of γ, we consider $1 \leq h \leq 2$ and $800 \leq Re \leq 2400$ which is well within the range where there is a unique stable steady flow.

We construct bifurcation diagrams in the (h,Re) parameter plane for fixed values of γ using the method of isoclines developed in [3], [4]. We briefly review the method here.

On a rectangular grid in the (h,Re) parameter plane with $\Delta h = 0.02$ and $\Delta Re = 10$ we perform simulations until a steady state is found. For each of the steady flow fields the ∞-isocline, defined as the set of points in the (r,z) domain where the radial velocity is zero, $u = 0$, is found. The set consists typically of a finite number of curves, and, in particular, the cylinder axis. Keeping track of the axial velocity w along the branches of the ∞-isocline allows us to locate stagnation points, as these are solutions to $w = 0$. A bifurcation function $G(h,Re)$ which measures the extremal value of w along a given branch of the ∞-isocline can be defined such that the creation or merging of stagnation points occurs when $G = 0$. Solving this equation yields the bifurcation curves in the (h,Re) plane. A simple alternative consists in plotting the ∞-isocline together with the 0-isocline (where $w = 0$) and monitor whether there are points of intersections of the two classes of isoclines.

Numerical results are shown in Fig. 3. For $\gamma = 0.075$, Fig. 3a, there is a parameter region with no secondary flow structure and a region with vortex breakdown. Crossing the bifurcation line between the two regions corresponds to crossing the line $c_1 = 0$ for $c_2 > 0$ in Fig. 2b. This bifurcation curve is associated with a simple degenerate stagnation point.

For $\gamma = 0.08$, Fig. 3b, there exists a narrow wedge in the parameter plane where a vortex ring exists. The wedge ends in a point corresponding to parameter values where a non-simple

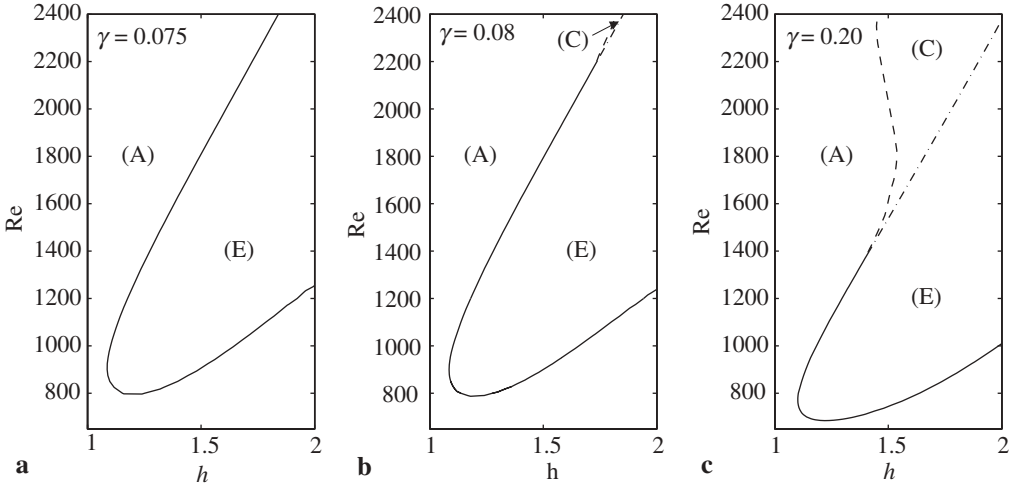

Fig. 3. Numerically obtained bifurcation diagrams; **a** $\gamma = 0.075$. **b** $\gamma = 0.08$. **c** $\gamma = 0.20$. The labels in each region correspond to the topologies in Fig. 1

degenerate stagnation point exists on the vortex axis. The local structure of the bifurcation diagram corresponds to Fig. 2b. No qualitative changes in the bifurcation diagrams occur as γ is increased. The double degenerate point moves into the diagram, and the wedge with a vortex ring grows considerably, as shown for $\gamma = 0.20$ in Fig. 3c.

4 Conclusions

In this paper we have shed light on the structure of vortex breakdown in a cylinder with rotating top and bottom in a parameter regime which has not been studied in systematic detail before. We have shown that for sufficiently large values of the rotation rate γ of the covers a secondary flow structure in the form of a vortex ring detached from the axis can occur. The parameter range in the (h, Re) plane where this flow topology occurs grows to a considerable size as γ is increased. To our knowledge, there are no experimental studies of the present parameter regime available in the literature, and the off-axis vortex ring has not previously been observed. However, for the flow in the cylinder where a thin rotating rod is added at the cylinder axis for control purposes, Husain et al. [14] interpret some of their visualization experiments as displaying an off-axis vortex ring.

The transition in Fig. 1 may be hard to detect experimentally. If the flow is visualized by tracer particles released close to the cylinder axis, the vortex ring will not be observed directly, unless it is very close to the axis. Hence, the transition may appear to consist of a direct transition from no vortex breakdown (Fig. 1a) to a large vortex breakdown bubble (Fig. 1e).

We have obtained topological bifurcation diagrams on the basis of the isocline method as a post-processing tool for numerical simulations. We have shown that the bifurcation diagrams are to be expected to appear close to non-simple stagnation points, and hence the computational results rest on a firm mathematical foundation.

References

[1] Bar-Yoseph, P., Solan, A., Roesner, K. G.: Numerical simulation and experimental verification of cavity flows. Lecture Notes in Mathematics **1431**, 229–235 (1988).

[2] Bessaï, R., Kadja, M., Eckhert, K., Marty, P.: Numerical and analytical study of rotating flow in an enclosed cylinder under an axial magnetic field. Acta Mech. **164**, 175–188 (2003).

[3] Bisgaard, A. V.: Structures and bifurcations in fluid flows with applications to vortex breakdown and wakes. PhD thesis, Department of Mathematics, Technical University of Denmark, 2005.

[4] Brøns, M., Bisgaard, A. V.: Bifurcation of vortex breakdown patterns in a circular cylinder with two rotating covers. To appear in Fluid Mech., 2006.

[5] Brøns, M.: Topological fluid mechanics of axisymmetric flows. In: Simulation and identification of organized structures in Flows (Sørensen, J. N., Hopfinger, E. J., Aubry, N., eds.), pp. 213–222. Dordrecht: Kluwer 1999.

[6] Brøns, M., Bisgaard, A.: Bifurcation of vortex breakdown patterns. In: Proceedings of the 2004 International Conference on Computational & Experimental Engineering & Sciences (Atluri, S. N., Tadeu, A. J. B., eds.), pp. 988–993. Georgia, USA: Tech Science Press 2004.

[7] Brøns, M., Voigt, L. K., Sørensen, J. N.: Streamline topology of steady axisymmetric vortex breakdown in a cylinder with co- and counter-rotating end-covers. J. Fluid Mech. **401**, 275–292 (1999).

[8] Brøns, M., Voigt, L. K., Sørensen, J. N.: Topology of vortex breakdown bubbles in a cylinder with rotating bottom and free surface. J. Fluid Mech. **428**, 133–148 (2001).

[9] Daube, O.: Numerical simulations of axisymmetric vortex breakdown in a closed cylinder. In: Vortex dynamics and vortex methods (Anderson, C. R, Greengard, C., eds.), Vol. 28 of Lectures in Applied Mathematics, pp. 131–152. American Mathematical Society 1991.

[10] Dusting, J., Sheridan, J., Hourigan, K.: Flows within a cylindrical cell culture bioreactor with a free-surface and a rotating base. In: Proceedings of the 15th Australasian Fluid Mechanics Conference (Behnia, M., Lin, W., McBain, G. D., eds.). University of Sydney 2004.

[11] Escudier, M. P.: Observations of the flow produced in a cylindrical container by a rotating endwall. Exp. Fluids **2**, 189–196 (1984).

[12] Gelfgat, A. Y., Bar-Yoseph, P. Z., Solan, A.: Steady states and oscillatory instability of swirling flow in a cylinder with rotating top and bottom. Phys. Fluids **8**(10), 2614–2625 (1996).

[13] Guckenheimer, J., Holmes, P.: Nonlinear oscillations, dynamical systems, and bifurcations of vector fields. New York: Springer 1983.

[14] Husain, H. S., Shtern, V., Hussain, F.: Control of vortex breakdown by addition of near-axis swirl. Phys. Fluids **15**(2), 271–278 (2003).

[15] Leibovich, S.: Vortex stability and breakdown: survey and extension. AIAA J. **22**(9), 1192–1206 (1984).

[16] Lim, T., Cui, Y.: On the generation of a spiral-type vortex breakdown in an enclosed cylindrical container. Phys. Fluids **17**, 044105-1–044105-9 (2005).

[17] Lopez, J. M.: Axisymmetric vortex breakdown, part 1. Confined swirling flow. J. Fluid Mech. **221**, 533–552 (1990).

[18] Okulov, V. L., Sørensen, J. N., Voigt, L. K.: Vortex scenario and bubble generation in a cylindrical cavity with rotating top and bottom. Eur. J. Mech. B **24**, 137–148 (2005).

[19] Peckham, D. H., Atkinson, S. A.: Preliminary results of low speed wind tunnel tests on a gothic wing of aspect ratio 1.0. Technical Report TN Aero 2504, British Aeronautical Research Concil CP508, 1957.

[20] Ronnenberg, B.: Ein selbstjustierendes 3-Komponenten-Laserdoppler-Anemometer nach dem Vergleichsverfaren, angewandt auf Untersuchungen in einer stationären zylindersymmetrischen Drehströmung mit einem Rückströmgebiet, Bericht 19. Göttingen: Max-Planck-Institut für Strömungsforschung 1977.

[21] Serre, E., Bontoux, P.: Vortex breakdown in a three-dimensional swirling flow. J. Fluid Mech. **459**, 347–370 (2002).

[22] Sørensen, J. N., Loc, T. P.: High-order axisymmetric Navier-Stokes code: description and evaluation of boundary conditions. Int. J. Num. Meth. Fluids **9**, 1517–1537 (1989).

[23] Sotiropoulos, F., Ventikos, Y.: The three-dimensional structure of confined swirling flows with vortex breakdown. J. Fluid Mech. **426**, 155–175 (2001).

[24] Spohn, A., Mory, M., Hopfinger, E. J.: Observations of vortex breakdown in an open cylindrical container with a rotating bottom. Exp. Fluids **14**, 70–77 (1993).
[25] Spohn, A., Mory, M., Hopfinger, E. J.: Experiments on vortex breakdown in a confined flow generated by a rotating disc. J. Fluid Mech. **370**, 73–99 (1998).
[26] Thompson, M. C., Hourigan, K.: The sensitivity of steady vortex breakdown bubbles in confined cylinder flows to rotating lid misalignment. J. Fluid Mech. **496**, 129–138 (2003).
[27] Valentine, D. T., Jahnke, C. C.: Flows induced in a cylinder with both end walls rotating. Phys. Fluids **6**(8), 2702–2710 (1994).
[28] Vogel, H. U.: Experimentelle Ergebnisse über die laminäre Strömung in einem zylindrischen Gehäuse mit darin rotierender Scheibe, Bericht 6. Göttingen: Max-Planck-Institut für Strömungsforschung 1968.

Authors' addresses: A. V. Bisgaard and M. Brøns, Department of Mathematics, Technical University of Denmark, Matematiktorvet, Building 303 (E-mail: m.brons@mat.dtu.dk); J. N. Sørensen, Department of Mechanics, Technical University of Denmark, Niels Koppels Allé, Building 403, DK-2800 Kongens Lyngby, Denmark